Eur. Phys. J. B (2026) 99:20
https://doi.org/10.1140/epjb/s10051-026-01143-0

THE EUROPEAN PHYSICAL JOURNAL B

Research - Condensed Matter

Numerical simulation on structural and topological transitions of GeO_2 liquid under compression

Emmanuel L. C. VI M. Plan[1], Haidang Phan[2], Hoang Anh Nguyen[3], Nguyen Van Hong[4], Pham Huu Kien[5], and Nguyen Van Yen[2,a]

[1] Faculty of Non-Traditional Security, Hanoi School of Business and Management, Vietnam National University, Hanoi 100000, Vietnam
[2] Faculty of Civil Engineering, VNU University of Engineering and Technology, Hanoi 100000, Vietnam
[3] Department of Geophysics, Colorado School of Mines, Golden, CO 80401, USA
[4] Faculty of Engineering Physics, Hanoi University of Science and Technology, Hanoi, Vietnam
[5] Thai Nguyen University of Education, 20 Luong Ngoc Quyen, Thai Nguyen, Vietnam

Received 22 October 2025 / Accepted 8 February 2026 / Published online 21 February 2026

Abstract. Molecular Dynamics simulation was performed to gain deeper insight on the effect of compression on liquid GeO_2, in particular on the transition between low-density phases to high-density phases. Similarities in the increase of GeO_x coordination number and the number of OGe_y links to the density increase allowed a characterization of the model densities at various values of pressure. The intermediate density phase displays not only an abundance in GeO_5 units but also the coexistence of at least two large GeO_x clusters of varying densities. Finally, the ring structures found in the regions of various densities suggest differing material properties that can arise from structural and topological heterogeneity. This work covers the gap on the effect of pressure on the micro-phase separation and ring structure in liquid germania.

1 Introduction

Network-forming oxides, such as silica (SiO_2) and germania (GeO_2), undergo structural and dynamical transformations under high pressure [1–21]. Higher values of pressure result in the shortening of bond lengths and an increase in coordination numbers (CN). GeO_2 systems under compression, in particular, have consistently displayed a shift from tetrahedral GeO_4 structural units to octahedral GeO_6 units, with the CN increasing from 4 to 6 [1, 11, 13, 14, 16]. This structural transformation at higher values of pressure is accompanied by characteristic changes in bond angular distributions [6, 8–10, 18].

Germania has often been examined and compared to silica owing to their structural similarities [5, 9, 17, 19, 22, 23]. Both GeO_2 and SiO_2 systems display tetrahedral units at ambient pressure and undergo transition to octahedral units. However, this transformation occurs at lower values of pressures in GeO_2, making it a useful analog for modeling high-pressure silicate behavior [5]. Despite having similar electronic density states, GeO_2 exhibits weaker bonds and smaller bond angles [23]. Differences also emerge in how pressures affect diffusion rates of these two oxides [9, 19].

Experimental studies of GeO_2 systems were constrained by instrumentation and pressure limitations. Techniques such as diffraction and fundamental spectral methods [11, 13, 24–27] have been used to calculate bond lengths, CNs, and oxidation levels, while spectroscopy [1, 14, 16, 28] can provide more information on bond angles and rings. In the past, pressures in the intermediate range of 8–44 GPa used to be considered state-of-the-art in laboratories [11, 25]; only recently have experts achieved higher pressures of at least 100 GPa [28, 29]. Complementing these efforts, simulations using molecular dynamics (MD) and ab initio techniques have extended analysis into regimes that remain experimentally challenging, providing predictive insight into more complex structural analyses or observation-intensive dynamical tracking and calculations [5, 9, 10, 12, 17, 19, 30–33]. For instance, void sizes in GeO_2 systems were quantified across various densities [10], while analyzing the movements of atoms enabled a microscopic description on atomic pathways in the formation of higher CN structural units [33].

Despite the growing number of studies on structural transitions in oxide systems, there remains a research gap for GeO_2 systems regarding the occurrence of micro-phase separation and its ring structure at high

[a] e-mail: nguyenvanyen@vnu.edu.vn (corresponding author)

pressure. Micro-phase separation has been reported for silicate systems [21] and results on ring structures are limited to the identification of dominant rings for specific cases [1, 34]. Recently, ring statistics and a Voronoi analysis were performed for a $MgSiO_3$ system, shedding light on how intermediate-range order results in secondary peaks at high pressure [35]. The effect of temperature on the structure of GeO_2 systems has been recently discussed [32], but the latest work on compressed liquid GeO_2 focused on molecular diffusion and dynamical heterogeneity [19]. In this work, we thus expound on the structural transformations of a liquid GeO_2 system, focusing on micro-phase separation occurring at intermediate values of pressure, and a more extensive thorough discussion on ring structures.

2 Methodology

We initialized a system consisting of 1833 Ge and 3666 O atoms randomly assigned in space and then heated up to 5000K. Then, the system was gradually cooled down to 3500 K at a rate of 2.5 K/ps. Our inhouse code uses the Verlet algorithm to evolve the numerical equation with a timestep of 0.48 fs. The Oeffner–Elliott (O–E) potential was used to calculate atomic interaction [9, 22, 36, 37].

After quenching, 13 different steady-state samples with varying pressures from 0 to 100 GPa were generated to analyze the effect of pressure. A target pressure P_0 was assigned for each sample, and an isotropic feedback barostat adjusts the simulation cell when virial pressure P deviates from P_0, i.e., every 1000 timesteps the simulation cell rescales isotropically if $|P - P_0| > \Delta P$ with $\Delta P = 10^{-4}$ GPa. Equilibration at each target pressure was performed in the NPT ensemble for 10^7 timesteps, after which statistics were collected from several annealing/production runs using more than 1000 configurations saved every 10 timesteps.

We first calculated the pair radial distribution function (PRDF) and the total distribution function of the system to examine the reliability of our model. The total distribution function is calculated from the pair distribution function $g_{ij}(r)$ according to following formula [15]:

$$g(r) = \frac{\sum_{i,\,j=1}^{n} c_i c_j b_i b_j g_{ij}(r)}{\sum_{i,\,j=1}^{n} c_i c_j b_i b_j}, \tag{1}$$

$g(r)$ where c_i is fraction of atom i (Ge or O) and b_i is its neutron scattering length ($b_{Ge} = 8.185$ fm, $b_O = 5.803$ fm) [38]. The structure factor $S(k)$ can then be calculated from the total distribution function (1) by performing Fourier transform [39]:

$$S(q) = 1 + 4\pi\rho \int_0^\infty [g(r) - 1] \frac{\sin(qr)}{qr} r^2 \mathrm{d}r, \tag{2}$$

where q is the scattering vector and ρ is the average atom number density.

Figure 1a shows the different PRDF of liquid GeO_2 at 0 GPa with the Ge–O PRDF displaying an initial peak at 1.74 Å, while the peaks of the Ge–Ge and O–O PRDFs are located at 3.32 and 2.82 Å, respectively, in excellent agreement with experiments [40, 41]. The first peak position of the total distribution function, which is strongly influenced by the peak in the Ge–O PRDF is also at 1.74 Å. The second peak is 2.88 Å, which was formed by the interplay of the peaks of the Ge–Ge and O–O PRDFs and damped by the low value of Ge–O PRDF. The structure factor of the GeO_2 liquid (Fig. 1b) is also in agreement with experiments [4], with deviations smaller than $2Å^{-1}$, and no major difference at the location of subsequent peaks and troughs were observed. Based on these, our GeO_2 liquid model is reliable and can be used to estimate other properties.

GeO_x clusters can be detected by first identifying seed Ge atoms with CN=x (i.e., with x O atoms within the cutoff distance). Each seed Ge atom and its neighboring O atoms form an initial cluster. Algorithmically, two clusters are merged if they share at least one common O atom, and the merging procedure is repeated until no any two cluster share a common O atom. These number of atoms in the final clusters can be used to obtain the cluster size distribution.

To analyze the ring structure, the no-shortcut criterion was used [35, 42, 43]. This algorithm treats the system as a network, where atoms are represented as nodes and links are edges. For any sequence of three connected nodes, the minimal cyclic path containing it is identified. Specifically, as provided in the appendix of [42], an exhaustive search of all cyclic paths containing these three connected nodes is performed, starting from potential three-node paths, four-node paths, and so on until a ring is identified. Any ring is validated to not have a path between any two nodes to be shorter than the path along the ring. When a ring is validated, all the ring is saved into a list. This process is done for each three connected nodes in the system. Finally, duplicate rings arising from various permutations of the same ring obtained from all possible three connected nodes are removed.

3 Results and discussion

3.1 Coordination number

We first report and confirm that our model reproduces the expected increase in coordination number (CN), correctly characterizing how pressure influences local GeO_2 structure and short-range order. The CN of an atom is the number of other atoms that are located within the distance from the central atom to the first minimum position of the PRDF; between Ge and O atoms this cutoff is $r_{Ge-O} \leq 2.36$ Å (Fig. 1a). Since the CN varies for each atom in a system, the CN for each

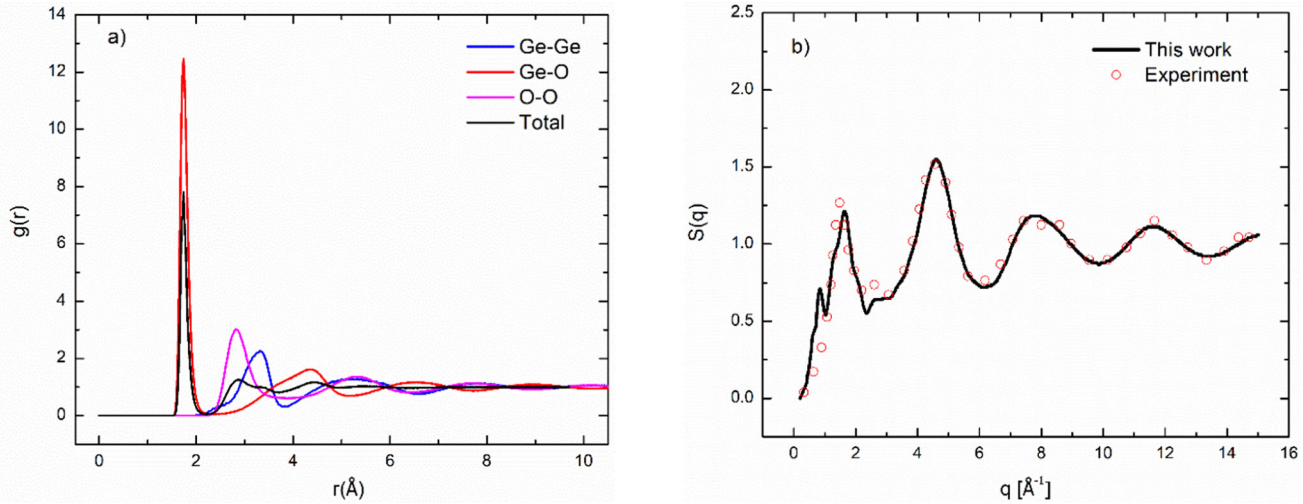

Fig. 1 **a** Calculated PRDF of Ge–Ge (blue), Ge–O (red), O–O (magenta) and the total distribution function of liquid GeO_2 (black); **b** structure factor for this study (solid line) and experiments (circles) [4]

type of atom was calculated as the average of all the CNs of atoms of that type.

As pressure increases, the atoms become more packed, increasing local density and leading to higher values of CN (Fig. 2a). The CN of Ge rapidly increases from around 4 to nearly 5.5 at 20 GPa, after which there is a slowdown in terms of increase from 40 to 60 GPa, and nearly stabilizing just below 6. Such a rapid increase in mean CN at low to intermediate values of pressure and a tapering increase at higher values is similar to experiments in amorphous GeO_2 and other simulations. Meanwhile, the mean number of Ge atoms of linked to O follows a similar shape, rising from 2.1 at 0 GPa to 2.7 at 40 GPa, and saturating below 2.8 GPa at 100 GPa (Fig. 2b). This progression shows that there is substantial molecular change from ambient pressure to intermediate values of pressure, diminishing increases starting from 20 GPa, and stabilization above 40 GPa.

Next, we analyzed the structural mapping of the CN with the units of the system and identify transitions between low-density (LD) and high-density (HD) configurations. The increase in CN is accompanied with structural change at the microscopic level, i.e., a CN of 4 defines a system composed predominantly of tetrahedral LD GeO_4 units, while a CN of 6 corresponds to that dominated by HD GeO_6 unit. Indeed, at ambient pressure, the predominant units are GeO_4 (95%), followed by GeO_5 (4.2%) and GeO_6 (0.8%) (Fig. 3a). We remark that the presence of non-tetrahedral units are consistent other numerical simulations at high temperature [8, 9]. As pressure increases, the system transforms from predominantly tetrahedral to octahedral network structure, with increasing CN. At 100 GPa, GeO_6 is most dominant (89%), with GeO_5 and GeO_6 accounting for 10% and 0.1%, respectively. The proportion of GeO_5 units increases at low pressure, reaches a maximum value of 43.9% at 15GPa, and decreases thereafter. This suggests that as pressure increases GeO_4 is converted to GeO_6 through the intermediate density (ID) state GeO_5.

GeO_x structural units are also connected through shared oxygen atoms between Ge atoms, coincidentally forming OGe_2 and OGe_3 links (Fig. 3b). The fraction of OGe_2 units is dominant at ambient pressure (hence CN is near 2), while at high pressure the fraction of OGe_3 units is very large at about 80%, aligned with the fact that CN≈2.8 (Fig. 2b). The transition on either GeO_x or OGe_y dominance occurs roughly at 15–20 GPa, when the number of GeO_5 units started to decline. This shift from low-to-high-density units is expected, since as pressure increases, molecular units become packed and forces molecules to adjust their structures.

3.2 Characterizing density

Given the clear structural evolution and density configurations at the local level, we next examine how these changes relate to the overall density of the system. Figure 4a shows the system density increases rapidly in a nearly linear manner before decelerating from 20 GPa. This shape interestingly resembles the increase in the number of OGe_3 subunits (Fig. 3b). The similarity suggests that the number of bonds connected to O at various values of pressure can be used to estimate the density ρ via the formula [21]:

$$\rho = \alpha\rho_{\mathrm{LD}} + (1-\alpha)\rho_{\mathrm{HD}}, \tag{3}$$

which is a weighted average of the densities at the lowest pressure value of 0 GPa ($\rho_{\mathrm{LD}} = 3.69\mathrm{g/cm}^3$) at and 100 GPa ($\rho_{\mathrm{HD}} = 6.55\mathrm{g/cm}^3$) and where α is the proportion of the OGe_2 links. The density calculated using (3), which assumes a linear combination of LD and HD values, provides an excellent estimate of pressures

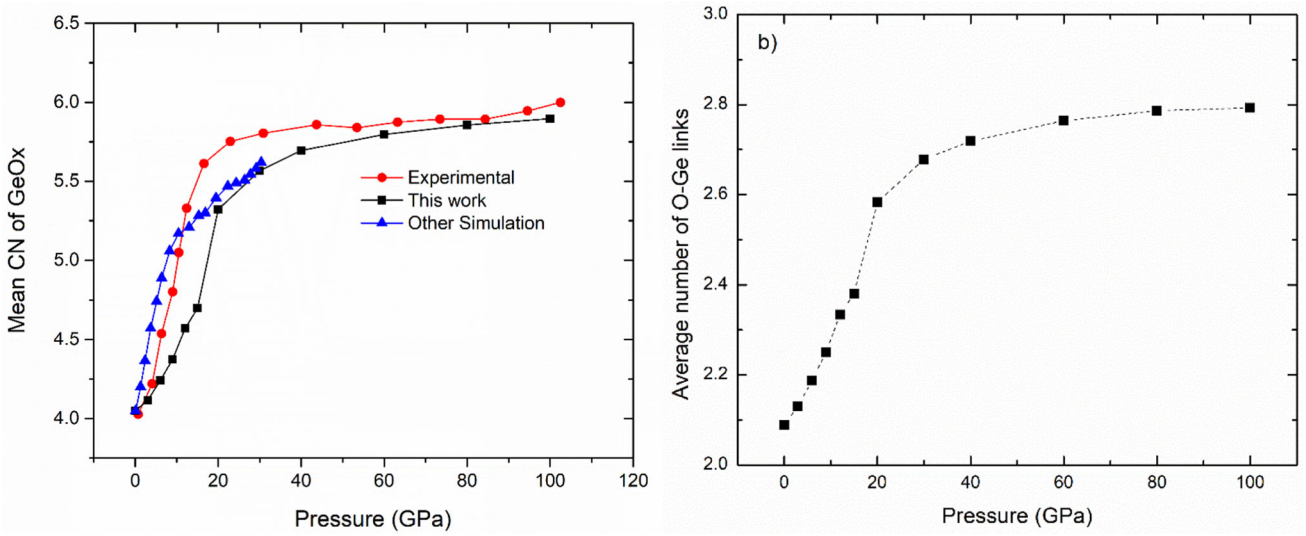

Fig. 2 **a** Coordination numbers of GeO_x in our simulations (square) with comparison to experiment (circle) [8] and other simulations (triangle) [29], and **b** average number of OGe_y links as a function of pressure

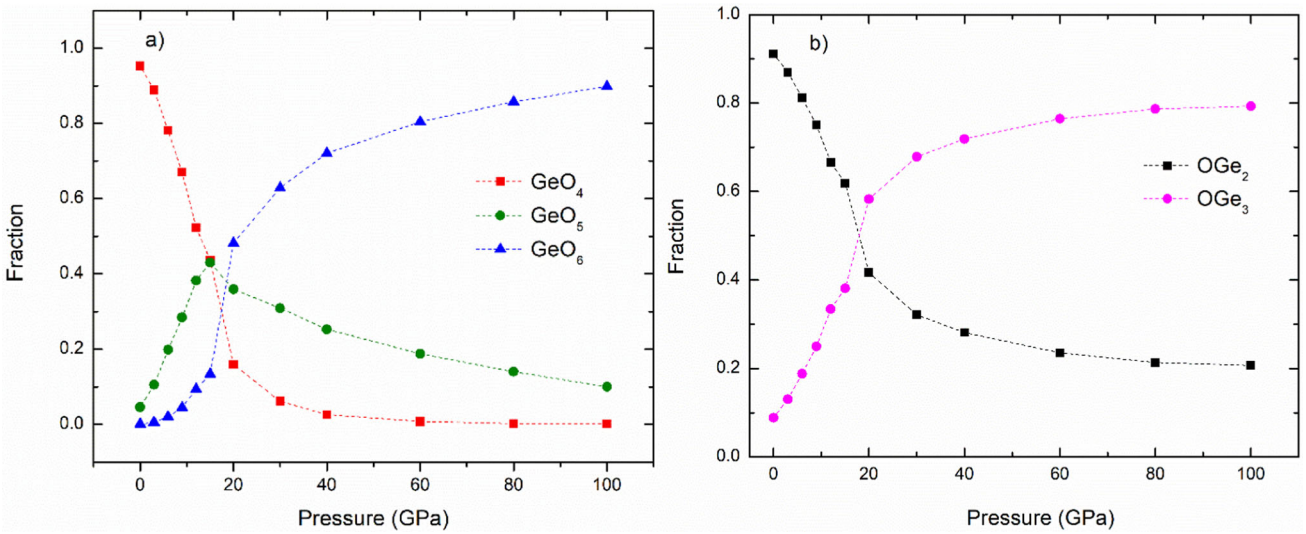

Fig. 3 Relative distribution of **a** GeO_x and **b** OGe_y structural units as a function of pressure

below 40 GPa (Fig. 4a). Above this value, the calculated density stagnates after 40 GPa, whereas the actual density continues to increase. The strong agreement at low–intermediate values of pressure suggests that the system density correlates with, the local densities governed by coordination numbers. However, the calculation based on oxygen linkages above raises a warning that such density estimates may only be valid for low-to-moderate densities. It may be possible to use the coordination number of Ge, but the intermediate stage via GeO_5 makes approximations at low pressure inaccurate, i.e., the number GeO_6 linkages does not increase as rapidly as the increase in density.

We also characterized the dependence of density on the CNs by providing an order parameter η through which we aim to define if the entire system has low or high density. For this, we use the number n_x of GeO_x units ($x = 4,6$) [30]:

$$\eta(\rho) = \frac{n_6 - n_4}{n_6 + n_4}. \tag{4}$$

Clearly, $|\eta| \leq 1$. When $n_6 = 0$, the dimensionless number $\eta = -1$, describing phases when mostly GeO_4 present; and when the system is mostly octahedral, then $\eta = 1$. This curve takes on values below -0.9 when $\rho \leq$

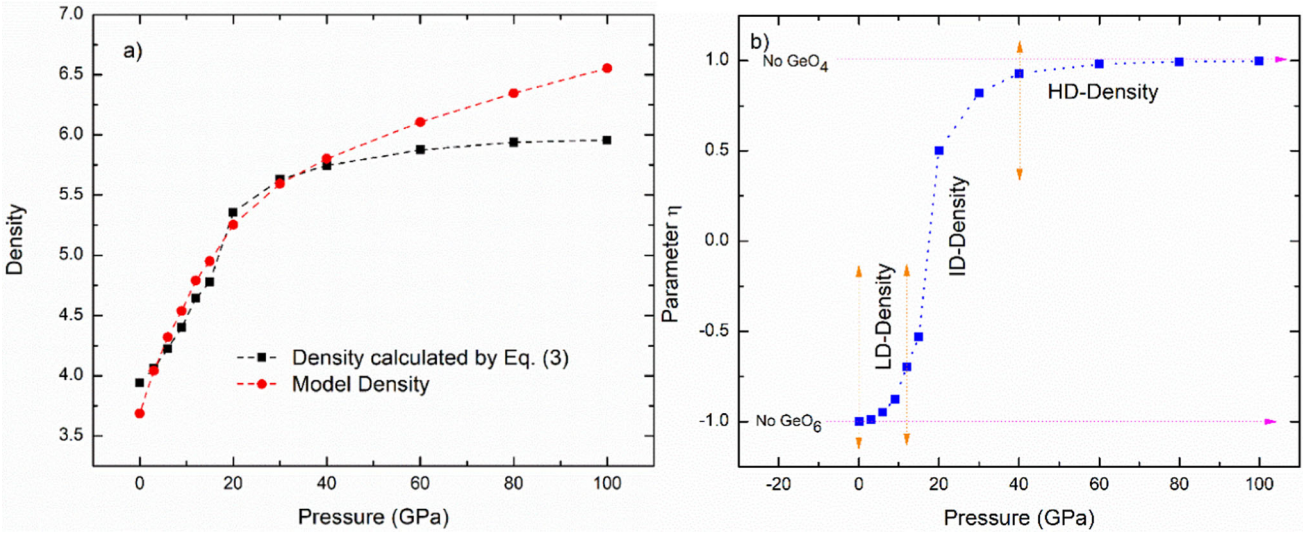

Fig. 4 **a** Density of the system as calculated by simulations (black) and as calculated by Eq. 3 (red). **b** Dimensionless number η as a function of pressure

12 GPa and exceeds 0.95 when $\rho > 40$ GPa (Fig. 4b). We can thus extend the definition of local density to the system density phases by dividing the η values into the following ranges:

- Low density (LD phase):$-1 < \eta < -0.9$
- Intermediate density (ID phase): $-0.9 < \eta < 0.95$
- High density (HD phase): $0.95 < \eta < 1$

The shape of η at various values of pressure (Fig. 4b) mimics the HD units in the system (Fig. 3a). At pressure values within the ID phase, more than one type of molecular structure is significantly present in the system, i.e., the proportion of GeO_x ($x = 5, 6$) units exceeds 0.25, whereas the number of GeO_4 units decrease. For values $-1 < \eta < -0.9$ (LD phase), the probability of finding the GeO_4 units is highest, indicating that the LD phase is primarily formed by LD units. The ID phase corresponds to $-0.9 < \eta < 0.95$, where the probability of finding a mix of different GeO_x units is highest and particularly the presence of GeO_5. For $0.95 < \eta < 1$ the probability of finding the GeO_6 coordination number is highest, and the number of LD and ID units have significantly diminished.

3.3 Microscopic phase separation

The discussion above shows how the overall system density increases with pressure nonlinearly and how the structural units rearrange when pressure increases. It does not reveal how the structural units are spatially arranged and clustered. To explore possible spatial heterogeneity, we now examine how GeO_x units cluster at different pressures.

Using model visualization, we have identified a sample of purely GeO_4 clusters (red), GeO_5 clusters (green) and GeO_6 clusters (blue) (Fig. 5). The dispersal of LD, ID, and HD regions in the model at the same pressure suggest microphase separation in intermediate values of pressure (15 GPa), meaning that all three density phases simultaneously exist in the model in different regions, i.e., the units do not convert from LD to ID to HD homogenously. Rather, units are more likely to transition to a denser phase when it is nearby an existing dense cluster. At higher values, less GeO_4 and GeO_5 units can be seen (40 GPa).

Figure 5 reveals evidence of micro-phase separation during the transition between LD and HD phases and how separate regions of various densities coexist, forming a heterogeneous network, and this can be quantified by examining cluster sizes, as shown quantitatively in Fig. 6 and illustrated in Fig. 7.

Clusters of varying densities and of different sizes appear across pressures. At 0 GPa, a large GeO_4 cluster with 5360 atoms exists, while only three GeO_6 cluster consists of 7 atoms (Fig. 5a). While the GeO_5 clusters are not negligible, they are small in size, with the largest containing 19 atoms. Thus, microscopic phase separation at 0 GPa is not observed. At 12 GPa, phase separation becomes apparent: two large GeO_4 (2841 atoms) and GeO_5 (3035 atoms) clusters are visible and pocket clusters of all densities are distributed. The pressure value of 15 GPa is unique among our models, because at this stage, there is a single dominant cluster of GeO_5 units (3360 atoms); the next biggest cluster is a GeO_4 cluster of 565 atoms. The conversion of GeO_4 and GeO_5 units to higher order units immediately proceed at 20 GPa, where a big GeO_5 cluster (296 atoms) coexists with a GeO_6 cluster (2685 atoms). At 40 GPa, there remain numerous GeO_4 clusters, while a large GeO_5 cluster (2001 atoms) and an even bigger GeO_6 cluster (4426 atoms) are present. Interestingly, there are only two HD clusters, suggesting that small HD regions quickly merged. Finally, at the extreme value of 100 GPa, only a handful of GeO_4 clusters exist with few

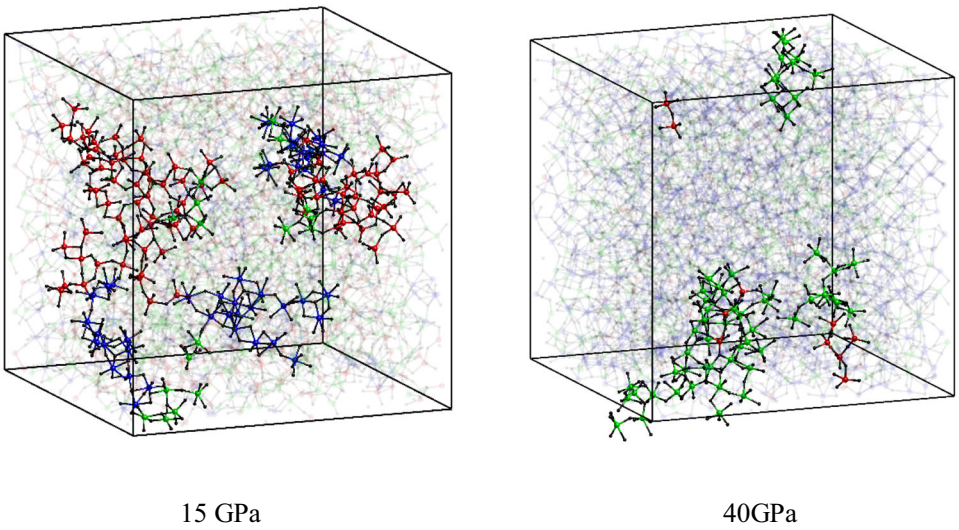

Fig. 5 Spatial distribution of clusters at 15 GPa and 40 GPa, showing GeO_4 clusters (red), GeO_5 clusters (green), and GeO_6 clusters (blue)

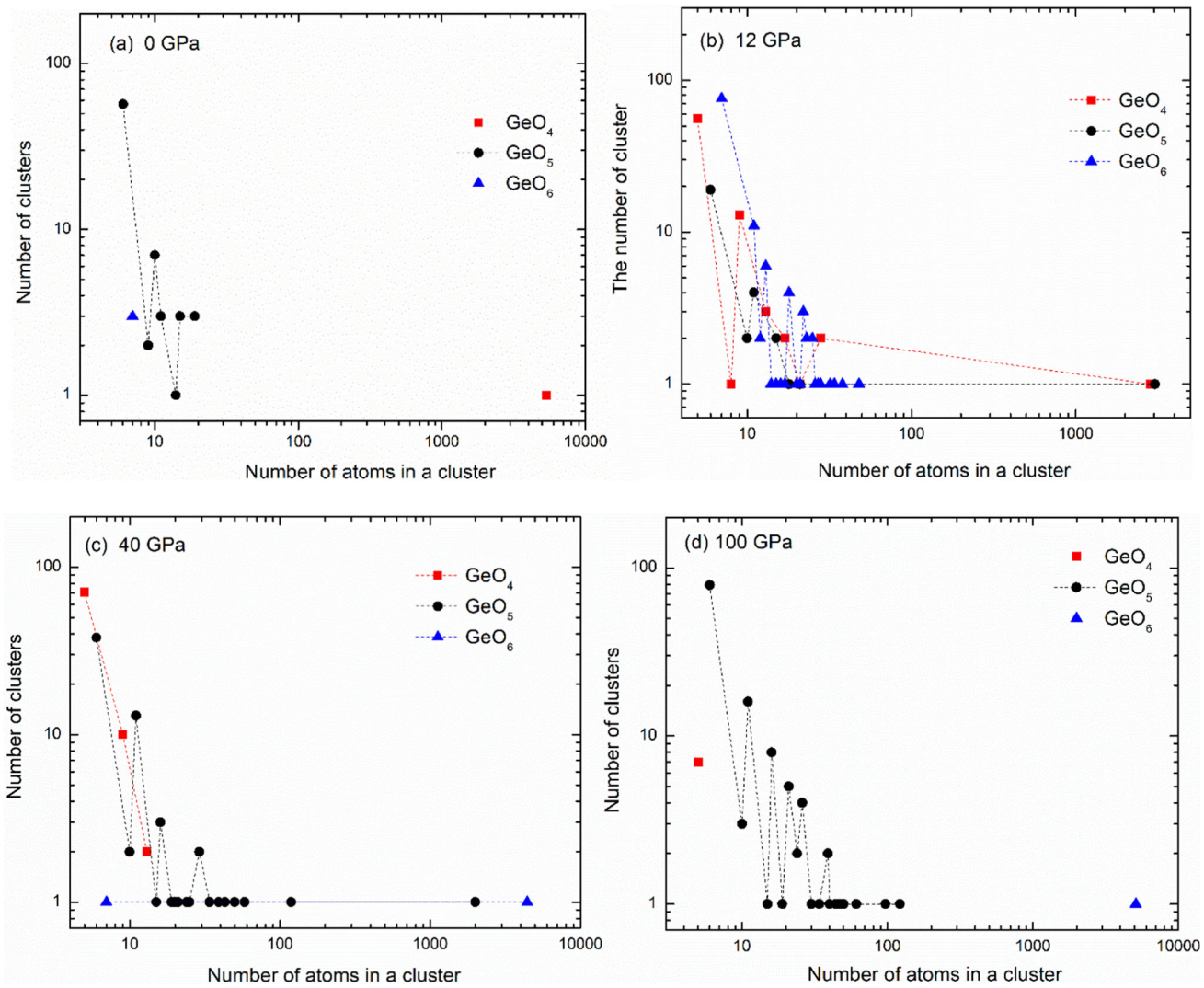

Fig. 6 Distribution of GeO_4, GeO_5, and GeO_6 clusters at various values of pressure

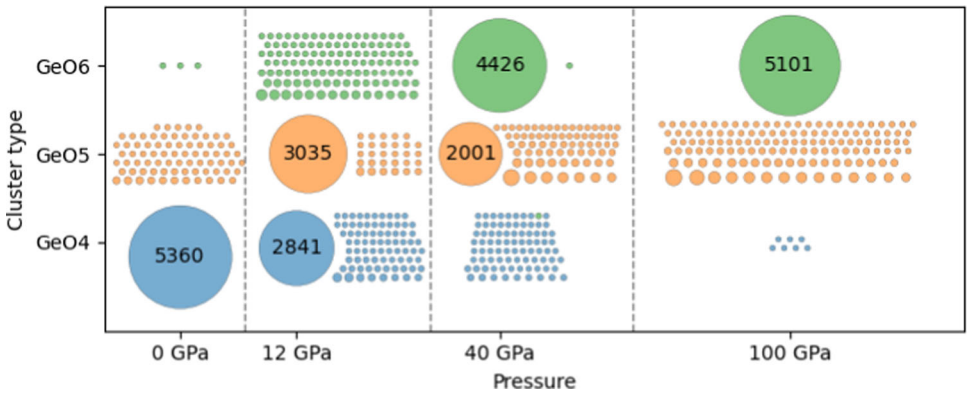

Fig. 7 Visualization of the cluster distribution (Fig. 6). Each cluster is represented by a circle, and the cluster size is represented by its size and the number, if present

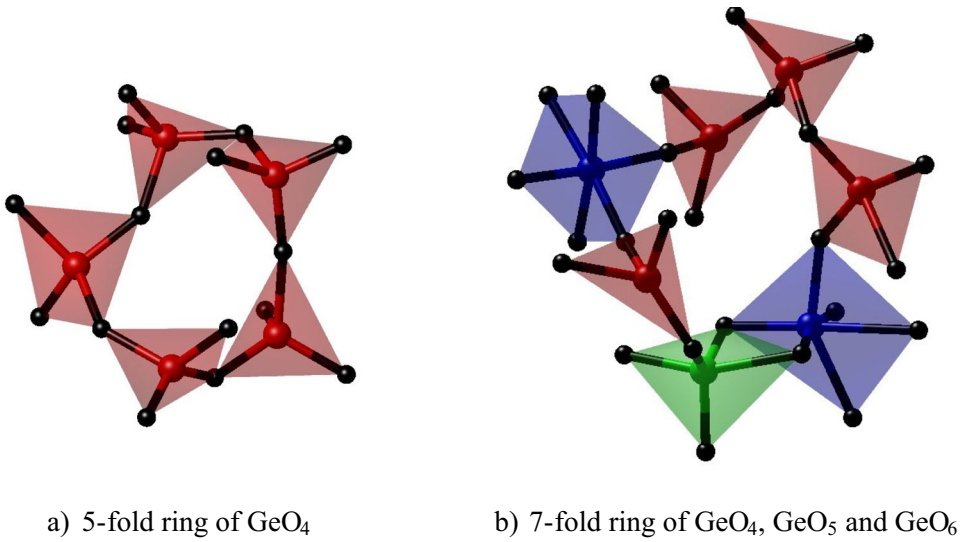

Fig. 8 Illustration of rings: **a** fivefold ring of GeO_4 and **b** sevenfold ring of GeO_4, GeO_5 and GeO_6

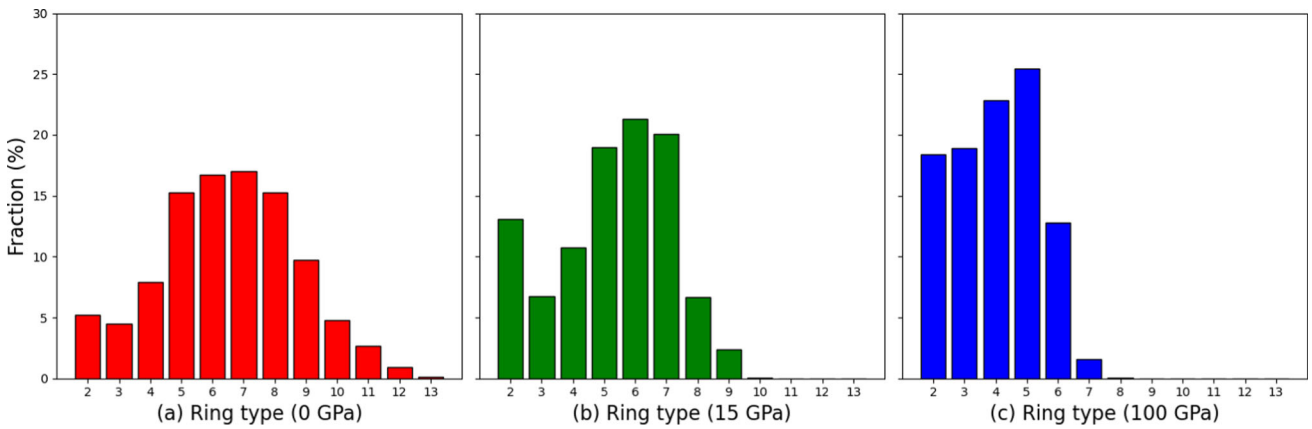

Fig. 9 Distribution of ring sizes at different pressures

atoms. One huge HD cluster (5101 atoms) exists, while several clusters of ID phases are scattered.

The main trend above is the formation of a large cluster of a specific phase that corresponds to the system density, i.e., a huge cluster of LD units is seen at low density, and a huge cluster of HD units is found at high density. This means that these units tend to form into one large cluster, although the formation of smaller clusters appear as well. Interestingly, GeO_5 clusters appear at all values of pressure, signifying the presence of high local density clusters at LD, and local regions of lower density at HD. Nevertheless, a large cluster of ID also appears when the system has ID. The ID phase is also characterized by the presence of another large cluster of LD GeO_4 or HD GeO_6 units. This suggests that, when increasing pressure, the large cluster of lower density does not transform collectively; rather, it is more likely that first, small regions of higher densities form, and then these small regions combine to make a new cluster of higher density; meanwhile, a large cluster

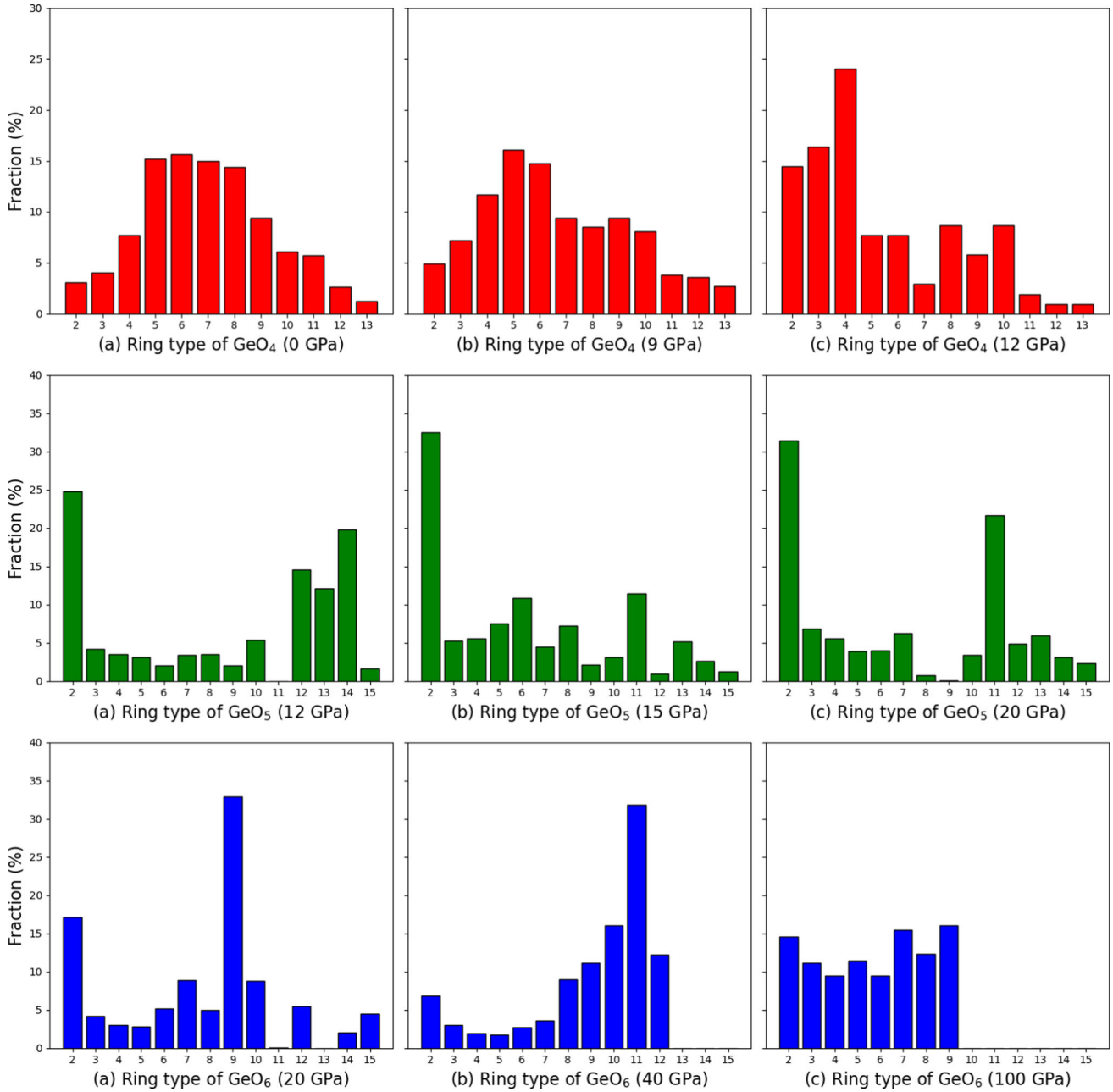

Fig. 10 Ring distribution of different GeO_x units at different values of pressure

of low density becomes smaller as its units transform to higher densities.

3.4 Ring structure

The effect of density on the formation of clusters of varying densities does not provide insights on the structural shape of the clusters. Large quantities of small rings will point to a more convex structure with less holes, while larger rings denote more chain-like formations. An n-fold ring of GeO_x units is a circular sequence of n units, connected via O atoms. In this work, we considered both rings made of units of various densities, i.e., for all $x = 4, 5, 6$, and rings consisting of a specific unit type. Figure 8 gives an illustration of such rings.

The distribution of rings at 0 GPa appears to have a Gaussian-like distribution from 2-folds to 13-folds, with a peak between 6 and 7 units (Fig. 9). As pressure increases, the clusters become tighter, resulting in smaller rings. The peak of the distribution shifts to the left. At the highest pressure considered in this study,

high-n n-fold rings are rare and small rings are most dominant: fivefold rings are most common (25.47% of all the rings), closely followed by fourfold rings.

Larger rings at lower pressures can be associated with a more open network topology in space. In contrast, a higher fraction of smaller rings at high pressure indicates a locally constrained and tightly connected structure. This suggests that high pressure germania may exhibit lower possibility of structural heterogeneity and topological rearrangement compared to the low density states. In addition, the smaller ring structures result in higher density, which contributes to a higher refractive index, altering the non-linear optical properties of the material. This insight is particularly valuable for the mechanical applications of GeO_2 material and their fabrication processes.

To elaborate on the ID phases with micro-phase separation, we study rings, where the units connected are of a specific GeO_x unit (Fig. 10). GeO_4 rings are typically normal at low pressure, with a shape not far from the overall ring distribution. As pressure increases toward the ID phase, the peak shifts toward smaller n, denoting smaller ring sizes. At this point, GeO_5 units start to appear and form rings. Interestingly, the ring distribution of ID units display more than one mode: one at $n = 2$ (denoting a small ring with a shared edge) and one at a much higher n. At 12 GPa, two large clusters are prominent: one LD (GeO_4) and one ID (GeO_5), and the LD (GeO_6) units have a ring distribution skewed to the right, while a significant portion of ID (GeO_5) rings have $n = 12, 13, 14$, accounting for a combined total of more than 25%. If small ring sizes are the signature of large dense spherical clusters, then high-n rings correspond to chain-like structures that have just begun to form a cluster. At slightly higher pressure 20 GPa, ID (GeO_5) and HD (GeO_6) units display a similar distribution: huge number of $n = 2$ rings and another peak at high n, with a difference on which peak is more prominent. In both cases, the rings suggest a presence of a dense cluster (contributing to a large value of twofold rings) and several less convex clusters external to it. Finally, GeO_6 rings display a large-n peak at moderately high values of pressure, approaching a nearly uniform distribution at 100 GPa.

4 Conclusion

Using molecular dynamics simulations, we investigated the structural evolution of liquid GeO_2 under compression. Our results showed a transformation from LD GeO_4-dominated configurations to HD GeO_6-rich structures with GeO_5 serving as an intermediate state at moderate values of pressure. This transition is accompanied by a rapid increase in density below 30 GPa and saturation afterward. Models based on OGe_y proportions or number of GeO_x ($x = 4, 6$) units were proposed to estimate the system density.

More interestingly, a spatial analysis of the atomic configurations revealed that the system exhibits micro-phase separation at intermediate pressures. Thus, instead of transforming homogenously, certain parts of the system display higher density than other parts. The shape of the local structures was also characterized via ring analysis, which showed a transition from large, flexible rings at low pressure to smaller rings at high pressure. This suggests that liquid germania at high pressure is highly densified, which limits local topological rearrangements.

Our work provided a detailed picture of structural and topological evolution of liquid germania at 3500 K and extreme values of pressure. A natural extension of this work is to examine the structural configurations and ring analysis in the high temperature–high pressure phase space. Since the melting point of GeO_2 is 1388 K [44], extending temperature alone from our current study of 3500 K may not result in drastic qualitative changes. Indeed, higher temperature may result in broader bond-length distributions, lower average coordination, and higher diffusion rates, as well as lower propensity to form large clusters and rings owing to higher disorder. It will nevertheless be interesting to see the temporal evolution of such clusters responding to the interplay of extreme pressure and temperature.

Experiments are, however, limited in such a regime, and numerical simulations may suffer theoretical limitations with regard to the optimal potential used in MD simulations. A potential approach here is to use ab initio MD, but the utilizing the appropriate system size and evolutional timescales will require large computing resources. Recently, machine-learning interatomic potentials have been used in classical MD simulation after being trained on data obtained from ab initio models [45–47]. In future work, employing such potentials would allow us to examine pressured-induced local and system structural configurations in extreme environments.

Acknowledgements This work has been supported/partly supported by VNU University of Engineering and Technology under project number CN25.03.

Author contributions

Emmanuel L. C. VI M. Plan and Nguyen Van Yen provided the main idea of this paper. Nguyen Van Hong and Pham Huu Kien performed the simulations. Hoang Anh Nguyen and Nguyen Van Yen performed some structural analysis. Haidang Phan, Nguyen Van Yen, Emmanuel L. C. VI M. Plan and Hoang Anh Nguyen analyzed the results and wrote, improved, and edited the manuscript.

Data availability statement This manuscript has no associated data or the data will not be deposited. [Authors' comment: This is a simulation study with no experimental data. All necessary data can be generated using the simulation details provided in the manuscript. Our processed data can be provided upon reasonable request.]

References

1. D.J. Durben, G.H. Wolf, Raman spectroscopic study of the pressure-induced coordination change in GeO_2 glass. Phys. Rev. B **43**(3), 2355 (1991). https://doi.org/10.1103/PhysRevB.43.2355
2. Y. Shimizugawa, F. Marumo, A. Nukui, K. Ohsumi, Anomalous scattering and EXAFS study of GeO_2–P_2O_5 glass system. J. Non-Cryst. Solids **176**(1), 76–84 (1994). https://doi.org/10.1016/0022-3093(94)90214-3
3. A.C. Wright, Neutron scattering from vitreous silica. V. The structure of vitreous silica: what have we learned from 60 years of diffraction studies? J. Non-Cryst. Solids **179**, 84–115 (1994). https://doi.org/10.1016/0022-3093(94)90687-4
4. S. Sampath, C.J. Benmore, K.M. Lantzky, J. Neuefeind, K. Leinenweber, D.L. Price, J.L. Yarger, Intermediate-range order in permanently densified GeO_2 glass. Phys. Rev. Lett. **90**, 115502 (2003). https://doi.org/10.1103/PhysRevLett.90.115502
5. M. Micoulaut, A comparative numerical analysis of liquid silica and germania. Chem. Geol. **213**(1–3), 197–205 (2004). https://doi.org/10.1016/j.chemgeo.2004.08.043
6. M. Micoulaut, Structure of densified amorphous germanium dioxide. J. Phys. Condens. Matter **16**(10), L131 (2004). https://doi.org/10.1088/0953-8984/16/10/L03
7. B.B. Karki, D. Bhattarai, L. Stixrude, First-principles calculations of the structural, dynamical, and electronic properties of liquid MgO. Phys. Rev. B **73**, 174208 (2006). https://doi.org/10.1103/PhysRevB.73.174208
8. K.V. Shanavas, N. Garg, S.M. Sharma, Classical molecular dynamics simulations of behavior of GeO_2 under high pressures and at high temperatures. Phys. Rev. B **73**(9), 094120 (2006). https://doi.org/10.1103/PhysRevB.73.094120
9. P.K. Hung, N.V. Hong, Simulation study of polymorphism and diffusion anomaly for SiO_2 and GeO_2 liquid. Eur. Phys. J. B. **71**(1), 105–110 (2009). https://doi.org/10.1140/epjb/e2009-00276-2
10. T. Li, S. Huang, J. Zhu, The structure and void analysis of pressure-induced amorphous GeO_2: molecular dynamics simulation. Chem. Phys. Lett. **471**(4–6), 253–257 (2009). https://doi.org/10.1016/j.cplett.2009.02.059
11. M. Baldini, G. Aquilanti, H.K. Mao, W. Yang, G. Shen, S. Pascarelli, W.L. Mao, High-pressure EXAFS study of vitreous GeO_2 up to 44 GPa. Phys. Rev. B **81**(2), 024201 (2010). https://doi.org/10.1103/PhysRevB.81.024201
12. D. Marrocchelli, M. Salanne, P.A. Madden, High-pressure behaviour of GeO_2: a simulation study. J. Phys. Condens. Matter **22**(15), 152102 (2010). https://doi.org/10.1088/0953-8984/22/15/152102
13. P.S. Salmon, J.W.E. Drewitt, D.A.J. Whittaker, A. Zeidler, K. Wezka, C.L. Bull, M.G. Tucker, M.C. Wilding, M. Guthrie, D. Marrocchelli, Density-driven structural transformations in network forming glasses: a high-pressure neutron diffraction study of GeO_2 glass up to 17.5 GPa. J. Phys. Condens. Matter **24**(41), 415102 (2012). https://doi.org/10.1088/0953-8984/24/41/415102
14. X. Hong, M. Newville, T.S. Duffy, S.R. Sutton, M.L. Rivers, X-ray absorption spectroscopy of GeO_2 glass to 64 GPa. J. Phys. Condens. Matter **26**(3), 035104 (2013). https://doi.org/10.1088/0953-8984/26/3/035104
15. M. Bauchy, Structural, vibrational, and elastic properties of a calcium aluminosilicate glass from molecular dynamics simulations: the role of the potential. J. Chem. Phys. **141**, 024507 (2014). https://doi.org/10.1063/1.4890083
16. J. Dong, H. Yao, Z. Guo, Q. Jia, Y. Wang, P. An, Y. Gong, Y. Liang, D. Chen, Revisiting local structural changes in GeO_2 glass at high pressure. J. Phys. Condens. Matter **29**(46), 465401 (2017). https://doi.org/10.1088/1361-648X/aa8d50
17. X. Du, J.S. Tse, Oxygen packing fraction and the structure of silicon and germanium oxide glasses. J. Phys. Chem. B **121**(47), 10726–10732 (2017). https://doi.org/10.1021/acs.jpcb.7b09357
18. S. Petitgirard, G. Spiekermann, K. Glazyrin, J. Garrevoet, M. Murakami, Density of amorphous GeO_2 to 133 GPa with possible pyritelike structure and stiffness at high pressure. Phys. Rev. B **100**(21), 214104 (2019). https://doi.org/10.1103/PhysRevB.100.214104
19. P.H. Kien, The structural phase-transition pathway under compression and dynamic properties in liquid GeO2. Mod. Phys. Lett. B **34**(17), 2050187 (2020). https://doi.org/10.1142/S0217984920501870
20. V.Y. Nguyen, E.L.C.V. Plan, H.K. Pham, A.T. Nguyen, V.H. Nguyen, H. Phan, Topological structural analysis and dynamical properties in MgSiO3 liquid under compression. Eur. Phys. J. B. **95**, 62 (2022). https://doi.org/10.1140/epjb/s10051-022-00313-0
21. V.H. Nguyen, H.A. Nguyen, Crystallisation of liquid silica under compression: a molecular dynamics simulation. Pramana **98**, 142 (2024). https://doi.org/10.1007/s12043-024-02839-7
22. M. Micoulaut, L. Cormier, G.S. Henderson, The structure of amorphous, crystalline and liquid GeO_2. J. Phys. Condens. Matter **18**(45), R753 (2006). https://doi.org/10.1088/0953-8984/18/45/R01
23. B. Walker, C.C. Dharmawardhana, N. Dari, P. Rulis, W.-Y. Ching, Electronic structure and optical properties of amorphous GeO_2 in comparison to amorphous SiO_2. J. Non-Cryst. Solids **428**, 176–183 (2015). https://doi.org/10.1016/j.jnoncrysol.2015.08.018
24. Y. Waseda, K. Sugiyama, E. Matsubara, K. Harada, Partial structural functions of GeO_2 glass determined by the anomalous X-ray scattering data coupled with neutron diffraction. Mater. Trans. JIM **31**(5), 421–424 (1990). https://doi.org/10.2320/matertrans1989.31.421
25. J.W.E. Drewitt, P.S. Salmon, A.C. Barnes, S. Klotz, H.E. Fischer, W.A. Crichton, Structure of GeO_2 glass at pressures up to 8.6 GPa. Phys. Rev. B **81**(1), 014202 (2010). https://doi.org/10.1103/PhysRevB.81.014202

26. Q. Mei, S. Sinogeikin, G. Shen, S. Amin, C.J. Benmore, K. Ding, High-pressure X-ray diffraction measurements on vitreous GeO_2 under hydrostatic conditions. Phys. Rev. B **81**(17), 174113 (2010). https://doi.org/10.1103/PhysRevB.84.174113
27. X. Hong, L. Ehm, T.S. Duffy, Polyhedral units and network connectivity in GeO_2 glass at high pressure: an X-ray total scattering investigation. Appl. Phys. Lett. **105**(8), 081904 (2014). https://doi.org/10.1063/1.4894103
28. G. Spiekermann, M. Harder, K. Gilmore, P. Zalden, C.J. Sahle, S. Petitgirard, M. Wilke et al., Persistent octahedral coordination in amorphous GeO_2 up to 100 GPa by K β'' X-ray emission spectroscopy. Phys. Rev. X **9**(1), 011025 (2019). https://doi.org/10.1103/PhysRevX.9.011025
29. Y. Kono, C. Kenney-Benson, D. Ikuta, Y. Shibazaki, Y. Wang, G. Shen, Ultrahigh-pressure polyamorphism in GeO_2 glass with coordination number >6. Proc. Natl. Acad. Sci. U. S. A. **113**(13), 3436–3441 (2016). https://doi.org/10.1073/pnas.1524304113
30. V.H. Vo, H.T.A. Nguyen, Z. Hoang, Liquid–liquid phase transition and anomalous diffusion in simulated liquid GeO2. Phys. B Condens. Matter **390**, 17–22 (2007). https://doi.org/10.1016/j.physb.2006.07.021
31. T.T. Duong, T. Iitaka, K.H. Pham, V.H. Nguyen, The first peak splitting of the Ge–Ge pair RDF in correlation to network structure of GeO_2 under compression. J. Non-Cryst. Solids **459**, 103–110 (2017). https://doi.org/10.1016/j.jnoncrysol.2017.01.003
32. M.T. Lan, T.T.H. Nguyen, V.H. Nguyen, K.H. Pham, Structure and dynamical heterogeneity in GeO2 liquid: a new approach. Eur. Phys. J. B. **92**(6), 1–7 (2019). https://doi.org/10.1140/epjb/e2019-100021-6
33. N.T.T. Ha, N.T. Trang, H.V. Hung, Correlation between microstructure and density of Germania melts: insight from molecular dynamics simulation. Indian J. Phys. (2021). https://doi.org/10.1007/s12648-020-01969-z
34. L. Giacomazzi, P. Umari, A. Pasquarello, Vibrational spectra of vitreous germania from first-principles. Phys. Rev. B **74**(15), 155208 (2006). https://doi.org/10.1103/PhysRevB.74.155208
35. H.A. Nguyen, V.H. Nguyen, Study of the structure of MgSiO3 system under compression by using ring statistics and voronoi analysis. Phys. Scr. **98**, 045919 (2023). https://doi.org/10.1088/1402-4896/acc5b7
36. R.D. Oeffner, S.R. Elliott, Interatomic potential for germanium dioxide empirically fitted to an ab initio energy surface. Phys. Rev. B **58**(22), 14791–14803 (1998). https://doi.org/10.1103/PhysRevB.58.14791
37. G. Guttierez, J. Rogan, Structure of liquid GeO_2 from a computer model. Phys. Rev. E **69**, 031201 (2004). https://doi.org/10.1103/PhysRevE.69.031201
38. V.F. Sears, Neutron scattering lengths and cross sections. Neutron News **3**(3), 26–37 (2006). https://doi.org/10.1080/10448639208218770
39. H. Nikoofard, T. Rezaye, A.H. Amin, The static structure factor of monatomic liquids using an analytical expression for the hard-sphere correlation function. Phys. Chem. **8**(4), 126–131 (2013)
40. D.L. Price, M.-L. Saboungi, A.C. Barnes, Structure of vitreous germania. Phys. Rev. Lett. **81**, 3207–3210 (1998). https://doi.org/10.1103/PhysRevLett.81.3207
41. C.E. Stone, A.C. Hannon, T. Ishihara, N. Kitamura, Y. Shirakawa, R.N. Sinclair, N. Umesaki, A.C. Wright, The structure of pressure-compacted vitreous germania. J. Non-Cryst. Solids **293**, 769–775 (2001). https://doi.org/10.1016/S0022-3093(01)00851-1
42. M. Matsumoto, A. Baba, I. Ohmine, Topological building blocks of hydrogen bond network in water. J. Chem. Phys. **127**(13), 134504 (2007). https://doi.org/10.1063/1.2772627
43. S. Le Roux, P. Jund, Ring statistics analysis of topological networks: new approach and application to amorphous GeS2 and SiO2 systems. Comput. Mater. Sci. **49**(1), 70–83 (2010). https://doi.org/10.1016/j.commatsci.2010.04.023
44. CAS Common Chemistry. (n.d.). Germanium oxide (GeO_2) (CAS RN 1310–53–8). CAS Common Chemistry. https://commonchemistry.cas.org/detail?cas_rn=1310-53-8. Accessed 28 Dec 2025
45. K. Matsutani, S. Kasamatsu, T. Usuki, Comparison of intermediate-range order in GeO_2 glass: molecular dynamics using machine-learning interatomic potential vs reverse Monte Carlo fitting to experimental data. J. Chem. Phys. **161**(20), 204103 (2024). https://doi.org/10.1063/5.0240087
46. H.T.T. Ta, M. Ferrario, S. Loehlé, M.C. Righi, Ab initio informed machine learning potential for tribochemistry and mechanochemistry: application for eco–friendly gallate lubricant additive. Comput. Mater. Today **1**, 100005 (2024). https://doi.org/10.1016/j.commt.2024.100005
47. X. Zhang, S.V. Divinski, B. Grabowski, Ab initio machine-learning unveils strong anharmonicity in non-Arrhenius self-diffusion of tungsten. Nat. Commun. **16**, 394 (2025). https://doi.org/10.1038/s41467-024-55759-w